Zinc stimulation of coastal productivity in low carbon dioxide environments

Riss M. Kell[1,2,+], Adam V. Subhas[2], Nicole L. Schanke[3], Lauren E. Lees[4], Rebecca J. Chmiel[1], Deepa Rao[1], Margaret M. Brisbin[2], Dawn M. Moran[2], Matthew R. McIlvin[2], Francesco Bolinesi[5], Olga Mangoni[5], Raffaella Casotti[6], Cecilia Balestra[7], Tristan J. Horner[2], Robert B. Dunbar[8], Andrew E. Allen[9,10], Giacomo R. DiTullio[3], Mak A. Saito[2*]

[1]MIT/WHOI Joint Program in Oceanography/Applied Ocean Science and Engineering, Woods Hole, MA 02543-1050 and Cambridge, MA, 02139-4307

[2]Department of Marine Chemistry and Geochemistry, Woods Hole Oceanographic Institution, Woods Hole, MA, 02543-1050

[3]Hollings Marine Laboratory, College of Charleston, Charleston, SC, 29424

[4]Department of Ecology and Evolutionary Biology, University of California at Irvine, Irvine, CA, 92697

[5]Dipartimento di Biologia, Università degli Studi di Napoli Federico II, Naples, Italy, 80138

[6]Stazione Zoologica Anton Dohrn, Naples, Italy, 80121

[7]Istituto Nazionale di Oceanografia e di Geofisica Sperimentale, Trieste, Italy

[8]Doerr School of Sustainability, Stanford University, Stanford, CA 94305

[9]Microbial & Environmental Genomics, J. Craig Venter Institute, San Diego CA, 92093

[10]Scripps Institution of Oceanography, Integrative Oceanography Division, University of California, San Diego, CA, 92037

*corresponding author, msaito@whoi.edu

[+]now affiliated with Gloucester Marine Genomics Institute, Gloucester MA, 01930-3006

Abstract

Zinc (Zn) is a key micronutrient used by phytoplankton for carbon (C) acquisition, yet there have been few observations of its influence on natural oceanic phytoplankton populations. In this study, we observed Zn limitation of growth in the natural phytoplankton community of Terra Nova Bay, Antarctica, due to low (~220 μatm) pCO_2 conditions, in addition to primary iron (Fe) limitation. Shipboard incubation experiments amended with Zn and Fe resulted in significantly higher chlorophyll *a* content and dissolved inorganic carbon drawdown compared to Fe addition alone. Zn and Fe response proteins detected in incubation and environmental biomass provided independent verification of algal co-stress for these micronutrients. These observations of Zn limitation under low pCO_2 conditions demonstrate Zn can influence coastal primary productivity. Yet, as surface ocean pCO_2 rises with continued anthropogenic emissions, the occurrence of Zn/C co-limitation will become rarer, impacting the biogeochemical cycling of Zn and other trace metal micronutrients.

Significance Statement

Zinc has tremendous nutritional importance in life, and due to its central role in carbon acquisition in major phytoplankton species, is directly connected to ocean carbon cycling. As a result, it has been hypothesized that co-limitation by zinc and CO_2 could influence primary productivity, but a connection between Zn and CO_2 had not yet been observed in field experiments. The present study demonstrates that Zn can be a limiting nutrient in natural waters, particularly in coastal environments where CO_2 is diminished by bloom events, and explores the implications for Zn-C co-limitation in the context of climate change: the oceans may have

decreased susceptibility to Zn-C co-limitations in the future due to the rapid input of anthropogenic CO_2 to the atmosphere.

Introduction

Primary productivity in the oceans is a key component of the global carbon cycle and is largely controlled by the availability of two macronutrients, nitrogen and iron (Fe). Yet there is increasing evidence that other elements or vitamins, such as phosphorus, cobalt (Co), or vitamin B_{12}, can also influence phytoplankton productivity, often as secondary limiting nutrients after nitrogen or Fe are added[1]. Zinc (Zn) can be scarce in the photic zone[2,3] where total dissolved Zn (dZn_T) can be as low as 0.1 nM in seawater due to biological uptake and complexation by organic ligands[4,5] which further lower Zn bioavailability[6–8].

Marine eukaryotic algae and copiotrophic bacteria possess a metabolic demand for Zn that is on par with that of Fe[6,9] and polar phytoplankton in particular may have an enhanced Zn demand based on genomic and laboratory analyses[10]. Yet there have been relatively few experimental studies examining the influence of Zn on natural phytoplankton communities **(Supplementary Table 1),** with findings that include negative results[11–13], slight Zn stimulatory results[14], Zn stimulation within Fe and Si uptake experiments[15], Zn primary and secondary limitation in the North Pacific in an unreplicated experiment[3], and secondary Zn limitation after primary Si limitation in the Costa Rica Dome[16]. Moreover, while low pCO_2 events are frequently observed in coastal environments due to high biological productivity[17–19], a connection between Zn and CO_2 had not yet been observed in field experiments, and it has remained unclear under what conditions Zn could act as a limiting oceanic micronutrient. However, a connection between cadmium (Cd; which can substitute for Zn when Zn is depleted[20]) and CO_2 has been

observed, with enhanced Cd uptake and particulate Cd in productive coastal Californian waters when exposed to lower pCO_2 conditions[21,22].

In contrast to the limited field evidence, laboratory studies have unequivocally demonstrated that marine phytoplankton are easily Zn-limited due to a large Zn requirement, and that this Zn limitation is exacerbated at low pCO_2[23,24] due to the use of Zn as a required catalytic cofactor within carbonic anhydrase (CA) metalloenzymes. CAs catalyze the reversible dehydration of HCO_3^- to CO_2, the substrate required by the carbon fixing enzyme RUBISCO. As HCO_3^- constitutes about 90% of the dissolved inorganic carbon (DIC) pool in the surface ocean, sufficient CA activity works to prevent carbon stress in marine phytoplankton by ensuring adequate CO_2 supply to RUBISCO. In some CA classes, the Zn cofactor can be substituted for by Co[25,26], and in some species, alternate CAs can be produced that use Cd or manganese (Mn)[27,28] as the cofactor, conferring a biochemical substitution flexibility with respect to metal availability known as cambialism[7].

In this study, we focused on Terra Nova Bay (TNB), located at the western edge of the Ross Sea, due to its history of large seasonal diatom blooms and resultant low pCO_2. The Ross Sea polynya has some of the highest abundances of phytoplankton in the world[29] and thus acts as a CO_2 sink during austral summer[30,31]. In the Ross Sea, dissolved iron (dFe) has been demonstrated to be the primary limiting nutrient for phytoplankton growth[12,32,33], and other micronutrients such as vitamin B_{12} and Mn have also been found to influence primary production rates and community composition here[34,35]. TNB has historically been found to be dominated by diatoms and the prymnesiophyte *Phaeocystis antarctica*[36,37]. Due to the high Zn and CO_2 demands of diatoms[23], TNB was selected as an ideal site to test for Zn/C co-limitation in the field.

Results and discussion

Biogeochemical characterization of Terra Nova Bay

We begin by biogeochemically characterizing the study site within Terra Nova Bay (TNB), Antarctica, which was temporally sampled for over one month (January 9 – February 18, 2018) during the 2017-2018 CICLOPS expedition **(Fig. 1a; Supplementary Table 2)** to concurrently characterize the natural phytoplankton bloom progression and biogeochemical changes in the water column. Low (~200 µatm) pCO_2 surface waters throughout TNB (**Fig. 1b**) made this an ideal site to investigate the presence of Zn/C co-limitation within the phytoplankton population.

TNB hosted a large phytoplankton bloom as indicated by high (> 3000 ng L^{-1}) chlorophyll *a* concentrations in January that waned into February (**Fig. 1c**). This phytoplankton community initially consisted of a mixed assemblage of both diatoms as indicated by fucoxanthin (fuco, **Fig. 1d**) and *Phaeocystis* as indicated by 19'-hexanoyloxyfucoxanthin (19'-hex, **Fig. 1e**). Surface fucoxanthin concentrations >200 ng L^{-1} were observed at the late TNB stations (**Fig. 1d**) while 19'-hex decreased to ~20 ng L^{-1} (**Fig. 1e**), indicating that the stations sampled in late February were dominated by diatoms rather than *Phaeocystis*. This was consistent with historical observations of phytoplankton succession patterns in TNB[36–38]. Pronounced and progressively deepening dZn_T depletion was observed in our temporal, upper water column sampling study of the TNB region spanning over a month (January-February 2018; **Fig. 1f**). dZn was depleted down to an average of 0.82 ± 0.47 nM at 10 m over all TNB stations with Zn-depleted areas of the water column progressively deepening to 50 m and then to ~100 m throughout January and February **(Fig. 1f)** indicative of strong Zn uptake and export from the

euphotic zone. Across all TNB stations, dFe_T in the upper 50 m remained below 1 nM (**Supplementary Figure 1a**) as observed previously in this region[39].

Temporal dynamics of the TNB bloom further showed that total Zn uptake (which was measured concurrently using a new stable isotope tracer method[40], see Methods) was highest in the shallow euphotic zone in early January and waned into February (**Fig. 1g**), following trends seen in chlorophyll *a* (chl *a*, **Fig. 1c**) and the phytoplankton pigments fucoxanthin (**Fig. 1d**) and 19'-hex (**Fig. 1e**), consistent with laboratory studies demonstrating the substantial Zn requirements of both diatoms and *Phaeocystis antarctica*[26,41]. Within TNB, a negative linear relationship between surface ($\leq$ 10 m) Zn uptake rates (ρZn) and surface (5 m) seawater pCO_2 partial pressure was observed (n = 15, R^2 = 0.63; **Fig. 1h**), consistent with an increased demand for Zn under low (220 μatm) pCO_2 as previously observed in Zn/C co-limitation experiments with phytoplankton in culture[23]. A positive linear trend (n = 27, R^2 = 0.87) comparing surface seawater pCO_2 and DIC concentrations confirmed that this was a primary productivity signal, with pCO_2 responding to DIC rather than alkalinity or salinity (**Supplementary Figure 2**).

Biogeochemical characterization of the incubation study site

We next describe the biogeochemistry of the water column at one TNB station (station 27, referred to as the "experimental site" herein) as this particular site was chosen for the shipboard incubation experiment (**Fig. 1a,b**; red star). This experimental site harbored a coastal bloom and was biologically and chemically characterized as having high *in situ* chlorophyll *a* levels (maximum of 3259 ng L^{-1} at 30 m; **Fig. 2a**), a substantial drawdown of surface seawater pCO_2 to 221 μatm (**Fig. 2b**) (a ~45% decrease compared to offshore waters in the Ross Sea measured during the same time frame; **Fig. 1b**), and a decrease in total dissolved inorganic carbon (DIC_T; 2186 μmol kg^{-1} at 5 m compared to the deep water (200-1065 m) average of 2224

± 2.1 μmol kg^{-1}**, Fig. 2c**). Within the water column, dZn demonstrated a pronounced decrease from 5.1 nM at 50 m to 0.9 nM at 10 m, representing an 82% decrease (and a 76% decrease comparing the minimum dZn_T value at 10 m to the average deepwater (210 – 1000 m) concentration of 3.9 nM ± 0.4; **Fig. 2d**), consistent with prior observations of surface dZn depletion in this region[39]. While Zn speciation was not measured in this study, it is possible that Zn organic complexation was present that prevented further depletion of Zn. A concurrent study of Co speciation observed complete complexation of dissolved Co in the upper water column in TNB, consistent with this idea[42]. Consistent with high macronutrient abundance in this region (as observed previously and in the present study; **Supplemental Figure 1b,c,d**), surface macronutrient concentrations (sum of nitrate and nitrite, phosphate, and silicic acid) were partially depleted at the experimental site with 64%, 46%, and 29% decreases in N+N, P, and Si, respectively, comparing 10 m and average deep water (200 – 1000 m) values (**Fig. 2e**). Measurements of high total Zn uptake at the experimental site were consistent with the observed dZn_T drawdown. Zn uptake was highest within the upper 50 m (46 pmol L^{-1} d^{-1} at 10 m) and decreased with depth (**Fig. 2f).**

Evidence for Zn stimulation of phytoplankton in shipboard incubations

An incubation experiment was conducted using surface waters (7 m) at the experimental site to examine controls on primary productivity, with triplicate treatments of Zn amended (+Zn; 2 nM as $ZnCl_2$), Fe amended (+Fe; 1 nM as $FeCl_2$), and Fe and Zn amended (+Fe+Zn) incubations, in addition to an unamended control. Significant differences in measured parameters among treatments are given in **Supplementary Table 3.** Addition of Fe alone (+Fe) resulted in significantly higher chl *a* content compared to controls (p = 9.5e-5) after six days (T6) (**Fig. 3a**),

demonstrating primary Fe limitation as observed previously in the Ross Sea[32,37]. However, addition of Zn alone (+Zn) also resulted in significantly higher chl *a* content compared to the control (p = 0.011), implying that a subset of the incubated phytoplankton population benefitted from the addition of Zn alone, without additional Fe, and was thus experiencing primary Zn limitation. The combined addition of +Fe+Zn resulted in the highest average chl *a* content among all treatments at T6, with 4.5 ± 0.21 μg L^{-1} compared to 3.9 ± 0.35 μg L^{-1} and 2.8 ± 0.15 μg L^{-1} achieved by +Fe and +Zn alone, respectively, demonstrating additive co-limitation between Zn and Fe[43]. Significant differences in seawater chemistry were also observed within these incubations over time, with larger decreases in DIC_T in all metal treatments compared to the control (-12.7 μmol kg^{-1} for +Fe (p = 5.3e-6), -8.2 μmol $kg^{-1}$for +Zn (p = 5e-5), and -18.5 μmol kg^{-1} for +Fe+Zn (p = 2.2e-16); **Fig. 3b**). The decrease in DIC_T observed with +Fe+Zn was significantly larger than that achieved with +Fe alone (p = 4.4e-3; **Fig. 3b**).

Algal Fe- and Zn-stress proteins within the experimental incubations provided additional independent lines of evidence corroborating the results described above. This included the detection of the recently described Zn/Co responsive protein ZCRP-A (a putative Zn chaperone)[44] as a biomarker of Zn stress as well as the iron starvation-induced proteins ISIP1A, ISIP2A and ISIP3 (ISIPs) as biomarkers of Fe stress (**Supplementary Table 4**). The ISIPs represent a group of unrelated proteins that are upregulated under Fe limitation in various algal species. ISIP1 proteins are responsible for endocytosis of siderophore-bound iron, ISIP2 proteins are involved in Fe^{3+} uptake, and ISIP3 has been suggested to act as an Fe storage protein[45,46]. Within the T6 incubation biomass, there was an increased abundance of ISIPs in the control and +Zn treatment and a corresponding decrease in ISIPs protein abundance within the +Fe and +Fe+Zn treatments, consistent with primary Fe limitation and the expected response to Fe

addition (**Fig. 3c**). ISIPs were taxonomically assigned to diatoms, *Phaeocystis*, and dinoflagellates (**Supplementary Figure 3a).** Similarly, we detected the presence of ZCRP-A in the T6 control, indicating the predilection for Zn limitation. The strongest expression of ZCRP-A was detected in the +Fe treatment (**Fig. 3c**) indicative of Fe addition driving the community towards increased Zn stress. Notably, ZCRP-A was still detected in the +Fe+Zn treatment (**Fig. 3c**), implying that the added Zn was unable to completely satiate Zn demand as phytoplankton biomass increased (as indicated by the increase in chl *a* at T6, **Fig. 3a**), despite added Zn (2 nM) being double that of added Fe (1 nM). Sequence analysis of the contigs identified as ZCRP-A homologs in these incubations revealed that all contigs contained one or more canonical conserved motifs found in COG0523 family proteins such as ZCRP-A (**Supplementary Figure 4 a,b)**. Coupled with evidence from prior laboratory studies[44], this provides further support for the role of ZCRP-A in responding to Zn scarcity.

ZCRP-A proteins were taxonomically assigned to chlorophytes, prasinophytes, dinoflagellates, and *Phaeocystis* (**Supplementary Figure 3a)**, with the detection of *Phaeocystis* ZCRP-A only in the +Fe treatment. The detection of ZCRP-A attributed to *Phaeocystis*, but the nondetection of ZCRP-A attributed to diatoms, implies that diatoms present were outcompeting *Phaeocystis* for Zn. In addition to these metal stress responsive proteins, variations in other functional proteins were observed among treatments. For example, RUBISCO and RNA polymerase were most abundant under +Zn+Fe conditions, and the latter was co-located within the same hierarchical cluster as ZCRP-A, consistent with their shared connection to cellular carbon metabolism (**Fig. 3c).** Our observations of Fe and Zn biomarkers shifting in abundance in response to their respective metal treatment provides independent evidence for Zn/Fe co-

limitation and verification that neither incubation treatment (+Zn nor +Fe) was contaminated with the other metal throughout the experiment.

Also consistent with these co-limitation observations in these incubations, the largest decreases in macronutrient (P and N+N) concentrations at T6 were observed in the +Fe+Zn treatment (**Supplementary Figure 5a,b**), as was the largest increase in particulate organic carbon (POC; **Supplementary Figure 5c**). POC collected from the +Zn and +Fe+Zn incubations was characterized by larger C:N atomic ratios (5.9 and 6.2, respectively) compared to the +Fe and T6 control (5.2 and 5.3; **Supplementary Figure 5d**) consistent with the stimulation of carbon uptake upon Zn addition alleviating carbon stress. Significantly higher bacterial abundances in both +Fe (p = 9.1e-4) and +Fe+Zn (p = 6.3e-4) treatments relative to the T6 control (**Supplementary Figure 5e**) indicated the alleviation of bacterial Fe limitation, consistent with prior reports[47]. Finally, photosynthetic efficiency of photosystem II (Fv/Fm) significantly increased with +Fe (p = 0.011) and with +Fe+Zn (p = 0.0036) at T4 (96 hours) compared to T4 controls, (note that there was no difference among treatments at T6) but did not significantly increase with +Zn alone, implying Fv/Fm may not be useful as a diagnostic for Zn stress and that caution should be used in interpreting its signals universally (**Figure 4j**).

Taxonomic characterization of incubation biomass via pigment analysis

The measurement of phytoplankton pigments over time within the shipboard incubations revealed a diverse taxonomic response to metal amendments, with less abundant phytoplankton groups responding most. Measured pigments included fucoxanthin (fuco), 19'-hexanoyloxyfucoxanthin (19'-hex), prasinoxanthin (prasino), chlorophyll *b* (chl *b*), and chlorophyll c3 (chl c3). Fuco is produced by both diatoms and by *Phaeocystis* under certain

conditions, while 19'-hex and chl c3 are indicative of *Phaeocystis* in this region[48]. Fuco:19'-hex ratios significantly increased in the +Fe (p = 4.2e-4) and +Fe+Zn treatments (p = 2.7e-3) (**Fig. 4a**) due to no significant change in fuco (**Fig. 4b**) and decreased 19'-hex (**Fig. 4c**) relative to the T6 control. *Phaeocystis* contributions to total fuco concentrations are typically minimal at the low Fe levels of the Ross Sea, though *Phaeocystis* can revert to making fuco rather than 19'-hex when released from Fe limitation[48], as was evident in these incubations by decreased 19'-hex:chl c3 ratios with +Fe and +Fe+Zn (**Fig. 4d**). *Phaeocystis* therefore likely contributed to total fuco by responding to Fe addition. Notably, significant decreases in both fuco:chl *a* and 19'-hex:chl *a* (**Fig. 4e,f**) in all treatments compared to the T6 control indicated that other phytoplankton groups contributed to chl *a* (**Fig. 3a**) without contributing fuco nor 19'hex. Increases in chl *b* (**Fig. 4g**) and prasinoxanthin (**Fig. 4h**) suggested that small green algae such as chlorophytes and prasinophytes also responded to +Fe and +Zn independently, consistent with the detection of chlorophyte ZCRP-A in these incubations (**Supplementary Figure 3a**).

Selective zooplankton grazing on small diatoms and solitary *Phaeocystis* cells may also have played a role in affecting phytoplankton biomass and the observed pigment:chl *a* ratios. For instance, higher ratios of phaeophytin:total phaeopigments were observed in +Fe and +Zn amended incubations (**Supplementary Figure 6a,b,c**) which may reflect grazing on solitary *Phaeocystis* cells, as high phaeophytin:total phaeopigments ratios were previously observed in *Phaeocystis* dominated waters of the Ross Sea[38].

We used metaproteomic data from T6 incubation biomass to supplement the pigment data and to further describe the major phytoplankton taxa present in the incubations at T6. Taxonomically assigned protein spectral counts were summed by genus, and indicated that *Phaeocystis*, diatoms, dinoflagellates, and cryptophytes were the most abundant phytoplankton

taxa as represented in the metaproteomic data, with cryptophytes, dinoflagellates, and *Phaeocystis* responding to metal treatments, consistent with the pigment results (**Fig. 4i).**

Detection of Zn- and Fe-stress protein biomarkers in the water column

Metaproteomic and metatranscriptomic analyses of the water column at the experimental site provided independent confirmation of the incubation results by demonstrating the occurrence of phytoplankton micronutrient Zn- and Fe- stress-response proteins naturally arising without influence from incubation conditions. In addition to ISIPs and ZCRP-A, we additionally detected ZCRP-B (a putative membrane-tethered Zn-binding protein)[44], Zrt/Irt-like (ZIP) Zn transporters, which are known to be used for Zn^{2+} and other divalent metal cation uptake in marine phytoplankton[45,49,50], and θ (theta) and δ (delta) carbonic anhydrases (CAs). θ-CAs with Zn^{2+} coordination sites have been documented in diatoms[51], including the polar diatom *Chaetoceros neogracile* RS19[52], but there are no studies to date investigating enzyme activity or efficiency with Co^{2+} or Cd^{2+}. In contrast, δ-CA (i.e, *Thalassiosira weissflogii* TWCA1) is known to function with either Co^{2+} or Zn^{2+} as a cofactor [53] conferring flexibility when Zn^{2+} is scarce.

Both proteins and transcripts of Fe and Zn stress biomarkers were observed throughout the water column. RUBISCO, ZCRP-A, and ISIP protein spectral counts within the 3μm size fraction were most abundant at the surface and decreased with depth (**Fig. 5a,b,d**), consistent with the depletion of trace metals in the photic zone due to high-biomass bloom conditions (**Fig. 1c)**. Throughout the water column, ISIPs were predominantly attributed to *Phaeocystis* and to the diatom genera *Fragilariopsis, Chaetoceros,* and *Pseudo-nitzschia* (**Fig. 5i, Supplementary Figure 7b**). ZCRP-A was detected in both 3 and 51 μm filter pore-size fractions (**Fig. 5b**) and was predominantly attributed to *Phaeocystis* (**Supplementary Figure 7c**). ZCRP-A transcripts

in the euphotic zone corresponded mainly to *Phaeocystis* and to the diatom genera *Chaetoceros* (**Fig. 5i**). We note that ZCRP-B, a protein also found to be upregulated in marine diatoms under low Zn/Co and characterized as a putative membrane-tethered Zn/Co protein ligand[44] was most abundant in the 0.2 μm fraction below 100 m (**Fig. 5c**). As ZCRP-B shares ~30% similarity to the bacterial ABC-type nickel transporter component NikA, spectral counts within the bacterial 0.2 μm fraction most likely reflect true bacterial NikA. BLAST analysis of all ZCRP-B contigs confirmed that all hits (across all size fractions) corresponded to bacteria (**Fig. 5i**).

ZIPs were almost solely found in the 51 μm fraction, likely due to the capture of abundant *Phaeocystis* colonies and chain-forming diatoms (**Fig. 5e; Supplementary Figure 7d**). The assignment of the majority of ISIPs and ZCRP-A proteins to *Phaeocystis* in the upper water column provides additional evidence that *Phaeocystis* was Zn/Fe co-limited at the study site, consistent with incubation results (**Fig. 3c, Supplementary Figure 3a**). The enhanced abundance of diatom θ-CA and δ-CA within the water column (**Fig. 5f,g**), as well as transcripts for the diatom Cd carbonic anhydrase CDCA, which can replace Zn^{2+} with Cd^{2+} as the catalytic cofactor[27], in the 3 μm and 51 μm fractions at 200 m (**Fig. 5h**) was indicative of the sinking of a prior diatom bloom event[54]. θ-CA and δ-CA were predominantly taxonomically assigned to the diatom genera *Pseudo-nitzschia* and *Chaetoceros*, respectively, while CDCA transcripts belonged to the diatom genera *Chaetoceros* and *Corethron* (**Fig. 5i**). The presence of θ-CA, but lack of δ-CA, assigned to *Chaetoceros* is consistent with proteomic analysis of the polar diatom *Chaetoceros neogracile* RS19 grown in culture under Zn limiting conditions[52].

Analysis of Zn/CO_2 growth limitation thresholds

In this study, we observed multiple independent lines of evidence that phytoplankton within incubation experiments and the field environment were experiencing Zn and Fe nutritional stress. Coupled with observations of greatly reduced C and Zn availability at the experimental site, which had nearly half the pCO_2 of atmosphere-equilibrated waters (221 μatm compared to ~420 μatm; **Fig. 1b, Fig. 2b**), and the greater demand for Zn as a catalytic cofactor within CAs that are required for CO_2 acquisition, TNB was likely experiencing Zn-C biochemically dependent co-limitation[7]. The low pCO_2 waters of the experimental site incubations naturally provided this low backdrop, allowing the stimulatory effects of Zn addition described above to be observed. This observation of Zn stimulation within low pCO_2 environments has not been observed previously, and these results imply that other highly productive coastal environments with low pCO_2 are also susceptible to Zn-C limitation, potentially limiting the extent of coastal phytoplankton blooms and carbon export.

Using the available quantitative constraints on Zn and CO_2 co-limitation thresholds available from the literature (see Methods), we estimated that the threshold for Zn-CO_2 limitation in algae occurs at 259 μatm pCO_2. We then compared this laboratory-determined Zn/C limitation threshold to both the *in situ* 221 μatm pCO_2 at our field study site, and to the historical, global trend in surface ocean pCO_2 (**Fig. 6**). It is evident that average, global surface ocean pCO_2 levels are rapidly rising above both the laboratory-estimated 259 μatm pCO_2 Zn/C limitation threshold and our field observation value of 221 μatm[55] (**Fig. 6a,b)** implying that over time, larger amounts of the surface ocean will cease to experience Zn/C limitation. In high-productivity regions, organisms may still experience Zn limitation (as shown in this study in TNB), but the fraction of the ocean that experiences these conditions will continue to shrink, alleviating Zn limitation and potentially increasing overall biological production. Though a fraction of the modern day surface

ocean, predominantly comprised of polar regions, is currently at ≤ 250 ppm pCO_2 (**Supplementary Figure 8a**), this represents a large decrease in oceanic extent compared to only 100 years ago (**Supplementary Figure 8b**). The continued rise in global pCO_2 levels as seen over the last ~100 years is potentially driving not only a shift away from Zn/C co-limitation, but also triggering broader changes in the biogeochemical cycling of Zn and other bioavailable trace metals within the oceans.

This study provides significant experimental field evidence using multiple independent lines of evidence (chlorophyll, DIC, Zn and Fe biomarker proteins), combined with contextual biogeochemical (pCO_2, dZn, and Zn uptake) and metaproteomic environmental data to demonstrate the presence of Zn limitation in Terra Nova Bay of the Ross Sea. Given the large Zn requirements of diatoms and other phytoplankton, it is perhaps surprising that more frequent positive observations of Zn nutritional effects have not been seen. We believe this is due to the combined challenges of avoiding Zn contamination and the need to initiate experiments in environments experiencing diminished pCO_2. Low pCO_2 conditions are well known to occur throughout coastal environments globally and could be further examined for Zn effects. While there are elaborate biochemical capabilities available to many marine algae for dealing with Zn scarcity[44], the geographic extent of Zn/C co-limitation will further decrease in the coming decades with rising anthropogenic CO_2 emissions. Despite this, the biochemical demand for Zn in marine organisms remains substantial, with cellular demand rivaling that of Fe. The multitude of metabolic functions requiring Zn, including but not limited to carbonic anhydrase activity, implies the need for further exploration of Zn influences in a changing ocean environment. Applying the protein biomarkers of Zn stress and threshold pCO_2 levels described in this study,

we now have an enhanced capability to predict the effect of Zn on marine productivity, particularly in dynamic and productive coastal waters.

Materials and Methods

Study area and sample collection

Sample collection occurred during the CICLOPS (Cobalamin and Iron Co-limitation of Phytoplankton Species) expedition (NBP18-01) aboard the RVIB *Nathaniel B. Palmer*, December 11, 2017 – March 3, 2018 in the Amundsen Sea and Ross Sea of the Southern Ocean (**Fig. 1a**). Station metadata is provided in **Supplementary Table 2.** All stations were assumed to be representative of TNB during this temporal study (as evident in the total dissolved metal, macronutrient, and chlorophyll *a* datasets). Water samples for dissolved trace metal analyses were collected using trace metal sampling protocols described previously[56]. A trace metal clean rosette suspended on a Kevlar line and equipped with twelve 8L X-Niskin bottles (Ocean Test Equipment) was used to collect seawater at depths ranging from 10 – 600 m. Niskin bottles were transported to a positive-pressure trace metal clean shipboard van for filtration upon surfacing. Total fluorescence on the vertical profiles was measured using an ECO chlorophyll fluorometer (Wet Labs) equipped to the rosette. The rosette also included instrumentation for measuring conductivity and temperature (Sea-Bird Electronics).

Preparation of plasticware

Polyethylene and polycarbonate sampling and incubation bottles were rigorously cleaned to remove trace metal contaminants before use. Bottles were rinsed with 18.2 Ω Milli-Q water (Millipore), soaked for 72h in <1% Citranox detergent, rotated, soaked for an additional 72h, and then rinsed five times with Milli-Q water. Bottles were then filled with 10% HCl (Baker instar-

analyzed) by volume and soaked for a minimum of one week, rotated, and soaked for another week. Bottles were then rinsed five times with dilute acid (HCl, pH 2) and stored double-bagged in plastic zip bags. All cleaning work was conducted in a Class 100 clean room.

Underway seawater pCO_2 partial pressure

Surface water pCO_2 measurements were conducted aboard the RVIB *Nathaniel B. Palmer* using an underway method consisting of an air-water equilibrator and IR CO_2 analyzer developed and operated by the Lamont-Doherty Earth Observatory (LDEO) group[57].

TDIC and POC measurements and calculation of pCO_2

Total alkalinity (TA) and dissolved inorganic carbon (DIC) were measured on CTD and incubations samples in near real-time aboard the NBP. Dissolved inorganic carbon (DIC) and total alkalinity (TA) samples were collected following the protocols of Dickson et. al 2007[58]. DIC analyses were conducted within ~4 h of collection. We acidified 1.25 mL of sample using an automated custom-built injection and bubble stripping system coupled to an infrared gas analyzer (LICOR LI7000) and integrated the infrared absorption signal versus time for each stripped gas sample to yield a total mass of CO_2. Each sample was analyzed in triplicate or greater. Since microbubbles regularly formed as samples warmed between sample acquisition and DIC analysis, every integration curve was visually inspected and those curves that exhibited evidence for bubbles were rejected. Certified reference materials (Dickson CRM batch 169) were analyzed between every 3 to 4 unknowns. The estimated precision based upon unknowns (>860 samples run in triplicate) and CRM replicates (n = 738) was ± 2.0 µmol kg^{-1} (±1 SD). As described by DeJong et al. 2015[59], analyses for TA on filtered samples were completed within ~12 h of collection by using a potentiometric titrator (Metrohm 855 Robotic Titrosampler). The

estimated precision based on replicate analyses of CRMs (n = 195) was ± 2.6 μmol kg^{-1} (±1 SD). DIC/TA pairs were used to calculate pCO_2 values using in situ temperature and salinity. Parameters were input to the MATLAB version of CO2SYS[60], and pCO_2 was calculated using the dissociation constants determined by the Dickson and Millero refit of Mehrbach's data (option 4).

We acknowledge offsets in seawater pCO_2 calculated from TA-DIC pairs and those measured using the ship's underway system. In general, values inferred from TA-DIC pairs are higher than underway measurements, sometimes by up to 70 ppm. Errors in acid dissociation constants due to temperature effects[61] cannot explain this offset, as using these updated constants only exacerbates the offsets rather than reconciling them. While these offsets are beyond the scope of the current manuscript, they hint at oceanographic effects on the carbonate system in very cold seas (e.g. large temperature gradients and their effect on the equilibration of the carbonate system). Nevertheless, both calculated and underway pCO_2 measurements are significantly below atmospheric CO_2 values, suggesting carbon limitation of the microbial community in Terra Nova Bay.

Analysis of historical atmospheric and surface ocean pCO_2 trends

Decadal surface ocean pCO_2 reconstructions from Jiang et al. 2023[55] were downloaded, binned by decade, and plotted using the 'violinplot' in MATLAB. Atmospheric pCO_2 data was assembled from the running Mauna Loa record[62], and from measurements made on Antarctic firn ice[63].

Calculation of Zn-and pCO_2 co-limitation of phytoplankton thresholds

There are few experimental measurements of Zn- and pCO_2-co-limitation, either in the lab or *in situ*. This study represents one of the first demonstrations of Zn- and pCO_2 co-limitation at a pCO_2 of ~220 ppm (Station 27, **Fig. 2b**). In the literature, several models exist to interpret co-limitation[7,64]. For this study we chose to use the biochemically dependent co-limitation model for growth rate (μ):

$$\mu = V_{max} \frac{[CO_{2(aq)}]}{\varphi K_s + [CO_{2(aq)}]}, \quad (1)$$

where V_{max} is the maximum growth rate, $[CO_{2(aq)}]$ is the aqueous CO_2 concentration of the growth medium in micromoles per kilogram of seawater, K_s is the half-saturation constant in micromoles per kilogram of seawater, and φ is a Zn-dependent growth term:

$$\varphi = \frac{[dZn] + K_{s,Zn}}{[dZn]} \quad (2)$$

Here, the dissolved Zn concentration in the growth medium [dZn] is modified by a Zn-dependent saturation constant ($K_{s,Zn}$). Few studies have enough experimental data to robustly establish a kinetic relationship between [dZn] and $[CO_{2(aq)}]$, so we compiled several estimates for these terms from the literature. Diatom growth rates under pCO_2 limitation were taken from Riebesell et al. (1993) [65]. Reported pH and temperature measurements for each treatment, a total alkalinity of 2300 μmol kg^{-1}, and a salinity of 35 were used to calculate aqueous CO_2 concentrations using CO2SYSv3.2.1.[66]. Reported V_{max} and K_s for *D. brightwellii, T. punctigera,* and *R. alata* were 1.46, 1.30, and 0.93 d^{-1}, and 1.4, 1.2, and 2.1 μmol kg^{-1}, respectively. Values for coccolithophore growth (K_s = 0.97 μmol kg^{-1}, V_{max} = 4.7 d^{-1}) were taken from Krumhardt et al. (2017) [67]. A value for $K_{s,Zn}$ of 300 pmol L^{-1} was taken from Buitenhuis et al. (2003). This value is for the coccolithophore *E. huxleyii* generated under varying CO_2 and Zn conditions, and Zn response

growth curves under single CO_2 conditions (ambient) are similar to other diatoms like *T. pseudonana*[68]. The value of 300 pmol L^{-1} appears high, but is tied to the functional form of the biochemically co-limitation equation[7,64]. Based on the same dataset and different models for co-limitation, Buitenhuis et al. (2003) arrived at $K_{s,Zn}$ values of ranging from 38 pmol L^{-1} to 300 pmol L^{-1}. They calculated Zn-limitation alone, at CO_2-replete conditions, of 19 pmol L^{-1}. Thus, the chosen value of $K_{s,Zn}$ is not a reflection of high Zn demand but determined by the functionality of biochemical co-limitation by Zn and C.

To calculate φ, a surface ocean Zn concentration of 50 pmol L^{-1} was assumed [2,69]. While these concentrations reflect total dissolved Zn, the relationship between bioavailable free Zn and dZn, especially in the field, remains unclear. Eq. 1 was then used to calculate effective CO_2 concentrations (and thus pCO_2 values) at which growth is halved, or in other words, $\mu = 0.5V_{max}$. We note that this calculation is distinct from the CO_2 half-saturation constant because of the co-limitation by Zn. The median pCO_2 threshold for 50% growth from the three diatom species was 278 ppm. Including coccolithophores decreases the median to 259 ppm. These values are slightly higher than the *in situ* evidence for Zn limitation at 220 ppm presented in the present study. Our results cannot be considered as an upper bound for Zn-CO_2 limitation, but serve as evidence for growth limitation under those specific environmental conditions.

Analyses of total dissolved metals using isotope dilution

The analysis of total dissolved metals has been described previously [70]. Briefly, seawater collected shipboard by pressure-filtering X-Niskin bottles through an acid-washed 142 mm, 0.2 µM polyethersulfone Supor membrane filter (Pall) within 3 hours of rosette recovery using high purity (99.999%) N_2 gas and stored at 4□C. All sample collection occurred shipboard within an on-deck trace metal clean van. Samples were acidified to pH 1.7 with high purity HCl (Optima)

within 7 months of collection and were stored acidified at room temperature for over 1 year prior to analysis.

Quantification of total dissolved Fe, Mn, Ni, Cu, Zn, and Cd was performed using isotope dilution. Acidified seawater samples were spiked with a stable isotope spike solution artificially enriched in ^{57}Fe, ^{61}Ni, ^{65}Cu, ^{67}Zn, and ^{110}Cd (Oak Ridge National Laboratory). Concentrations and spike ratios were verified by ICP-MS using a multi-element standard curve (SPEX CertiPrep). Preconcentration of spiked seawater samples for total dissolved metal analysis was performed using the automated solid phase extraction system seaFAST-pico (Elemental Scientific) in offline concentration mode with an initial volume of 15mL and elution volume of 500µL [71,72]. Following preconcentration, multielemental quantitative analysis was performed using an iCAP-Q inductively coupled plasma-mass spectrometer (ICP-MS) (Thermo Scientific). Concentrations of Mn, Fe, Ni, Cu, Zn and Cd were determined using a six-point external standard curve of a multi-element standard (SPEX CertiPrep), diluted to range from 1-10 ppb in 5% nitric acid. An indium standard (SPEX CertiPrep) was similarly added to these standard stocks, diluted to range 1-10 ppb. Instrument injection blanks consisted of 5% nitric acid in Milli-Q. Standard curve R^2 values were ≥0.98 for all metals monitored. Method accuracy and precision were assessed using the 2009 GEOTRACES coastal surface seawater (GSC) standard (n = 8; **Supplementary Table 5**), which produced values consistent with consensus results.

Macronutrient, pigment, and Fv/Fm analyses

Seawater for macronutrient (silicate, phosphate, nitrate, and nitrite) analyses were filtered through 0.2 µm pore-size Supor membrane filters and frozen at sea in acid-washed 60-mL high-density polyethylene bottles until analysis. Macronutrient analyses were conducted by nutrient

autoanalyzer (Technicon Autoanalyzer II) by Joe Jennings at Oregon State University. The chemotaxonomic distribution of phytoplankton pigments was determined using HPLC as described previously[73]. Photosynthetic efficiency of photosystem II (Fv/Fm) was measured using a Phyto PAM phytoplankton analyzer (Walz, Effeltrich, Germany) as described previously[74].

Bacterial abundance

One ml samples for heterotrophic prokaryotes abundance (HPA) analysis were fixed for 10 min with a mix of paraformaldehyde and glutaraldehyde (1% and 0.05% final concentration, respectively), frozen in liquid nitrogen and stored at −80°C until analysis. After thawing, samples were stained with SYBR Green (Invitrogen Milan, Italy) using 10^{-3} dilution of stock solution for 15 min at room temperature. Cell concentrations were assessed using a FACSVerse flow cytometer (BD BioSciences Inc., Franklin Lakes, USA) equipped with a 488 nm Ar laser and standard set of optical filters. FCS Express software was used for analyzing the data and HP were discriminated from other particles on the basis of scatter and green fluorescence from SYBR Green [75].

Zn uptake rates using ^{67}Zn.

^{67}Zn stable isotope uptake experiments were performed to quantify the movement of dissolved Zn to the particulate phase (in units of pmol L^{-1} d^{-1}). Briefly, raw (unfiltered) seawater was collected using the trace metal rosette over a depth range of 10 – 600 m into 250mL trace metal clean polycarbonate bottles. Bottles were spiked with ^{67}Zn such that the total added (spiked) concentration of Zn was 2 nM. Immediately after spiking, incubation bottles were sealed, inverted to mix, and transferred to flow-through on-deck incubators for 24hr. Biomass was collected after 24hr by vacuum filtering each incubation sample at 34.5 kPa (5 psi) onto an

acid-cleaned 3μm pore-size acrylic copolymer Versapore filter (Pall) mounted on an acid-cleaned plastic filtration rig. Sample filters were retrieved from storage at -80°C, removed from cryovials using plastic acid-washed forceps, and transferred into trace metal clean 15 mL PFA vials with 4 mL of 5% HNO_3 (Optima) containing a 1 ppb Indium (In) internal standard. Filters were digested for ~3.5h at 140°C using a HotBlock® heating block (Environmental Express, USA) before they were removed and discarded. After evaporating the remaining solution to just dryness, the residue was resuspended in 2 mL of 5% HNO_3 (Optima) by light vortexing. Process blank filters were digested and processed as sample filters were. Digests were analyzed in duplicate by ICP-MS using a Thermo ICAP-Q plasma mass spectrometer calibrated to a multi-element standard curve (Spex Certiprep) over a range of 1 – 20 ppb. Natural Cd and Zn isotope abundances of the standards were assumed to calculate concentrations of ^{110}Cd, ^{111}Cd, ^{114}Cd, ^{67}Zn, ^{66}Zn, and ^{68}Zn. Total Zn uptake (pmol L^{-1} d^{-1}) was calculated using particulate ^{67}Zn and total water column dZn measurements as described previously[76]. Particulate metal measurements are inclusive of 1). active transport of metal into cells, 2). nonspecific metal adsorption to cell surfaces, 3). metal adsorption to non-living particulate organic matter, and 4). metal adsorption to particulate inorganic matter, though we expect active transport into cells to dominate the measured particulate isotopic signal due to the high abundance of actively growing autotrophic cells in the photic zone observed in Southern Ocean during austral summer.

Shipboard incubation experiments

Incubation experiments were conducted at station 27 (-74.9870°N, 165.8898°E). Raw surface seawater was pumped directly into a cleanroom container van, collected into acid-cleaned 50L carboys, and dispensed into acid-washed 1L polycarbonate bottles using a trace

metal sampling system with acid-washed polypropylene tubing and a teflon diaphragm pump. Incubation bottles were first rinsed with seawater then filled. Seawater was collected at 16:05 UTC. Triplicate incubation bottles were amended with +Fe (1 nM), +Zn (2 nM) and +Fe+Zn, sealed, and placed into a flow-through on-deck incubator with light screens that shaded the incubator to 20% percent ambient surface irradiance. Incubations were sampled at 0, 48, 96, and 144 hours (corresponding to T0, T2, T4, and T6 timepoints) for analysis by filtering onto GFF filters for chlorophyll (all time points, biological triplicates), pigment analyses (T6, biological triplicates), and proteomic analyses (T6, pooled biological triplicates). Chlorophyll was extracted immediately, otherwise samples were frozen at -80°C until further analyses, with pigment and protein samples kept in -80°C freezers, liquid nitrogen dewars, or dry ice coolers at all times during transport back to the laboratories. All amendments and sampling were conducted in a positive-pressure, clean room van with laminar flow hoods and plastic sheeting to minimize trace-metal contamination.

Metaproteomic analysis

Water column metaproteomic biomass was collected onto 0.2, 3, and 51 µm pore-size filters using in-situ battery operated McLane pumps. Incubation metaproteomic samples were collected on GFF filters as described above. Filters were frozen at -80°C and transported as described above until laboratory extractions. Frozen filters were thawed and extracted as described previously [77]. Briefly, filters were extracted using SDS detergent to solubilize both membrane and soluble proteins and subjected to a 10-min heating incubation at 95 °C. Protein material was subsequently purified, alkylated, reduced and digested with trypsin (mass spectrometry grade; Promega Corporation) at a trypsin:protein ratio of 1:20 and peptides were

purified using C18 tips (Pierce C18 Tips, 100-µl bed; Thermo Fisher Scientific). Purified peptides were diluted to 0.1 µg $µl^{-1}$ and 20 µl (2 µg) was injected onto a Dionex UltiMate 3000 RSLCnano LC system (Thermo Fisher Scientific) with an additional RSLCnano pump run in online two-dimensional active modulation mode coupled to a Thermo Fusion Orbitrap mass spectrometer.

A translated metatranscriptome (see below) was used as a reference protein database and peptide spectra matches were performed using the SEQUEST algorithm within Proteome Discoverer v.2.1 (Thermo Fisher Scientific) with a fragment tolerance of 0.6 Da and parent tolerance of 10 ppm. Identification criteria consisted of a peptide threshold of 95% (false discovery rate (FDR) = 0.1%) and protein threshold of 99% (1 peptide minimum, FDR = 0.8%) in Scaffold v.5 (Proteome Software) resulting in 5,387 proteins identified in the incubation experiment and 27,924 proteins identified in the water column. To avoid double-counting mass spectra, exclusive spectral counts were used for the downstream proteomic analysis. Exclusive spectral counts were normalized using the normalized spectral abundance factor (NSAF) calculation [78] to allow for a comparison of protein abundance across samples while remaining consistent with the metatranscriptomic procedure, see Cohen et al. 2021 for details. Counts associated with redundant ORFs (sharing identical taxonomic and functional assignments) were summed together.

Relative abundances of *Phaeocystis*, cryptophytes, dinoflagellates, and diatoms ("major groups") within the T6 incubation biomass were estimated by summing exclusive total protein spectral counts across all detected proteins that were assigned to the same group (as noted by best hit species; see metatranscriptomic methods below). Protein hits with LPI scores < 0.5, low assigned species identity (< 50%), or no assigned species were excluded.

Metatranscriptomic analysis

RNA sequencing was performed using the Illumina HiSeq platform. Transcriptomic assemblies were generated for biomass collected using McLane pumps filtered through 0.2, 3, and 51 μm pore-size filters. In order to enrich metatranscriptomic libraries derived from 0.2 μm filters in prokaryotic transcripts and libraries derived from 3 μm and 51 μm filters in eukaryotic transcripts, 0.2 μm libraries were generated from total rRNA-depleted mRNA and 3 μm and 51 μm libraries were generated from polyA mRNA. Total RNA was extracted from 0.2 μm, 3 μm, and 51μm filters using Macherey-Nagel a NucleoMag RNA kit (Macherey-Nagel GmbH & Co.KG). Cleared lysate was loaded into a 96 deep-well plate and put on an epMotion 5075 TMX liquid handler to complete the RNA extraction following the Machery-Nagel standard protocol. For 3 μm and 51 μm samples with total RNA greater than 1 ug, 800 ng of total RNA was used for preparing poly A libraries with an Illumina Stranded mRNA Prep Ligation kit (Illumina), following the manufacturer's protocol. For the 3 μm and 51 μm samples with total RNA less than 1 ug, 20 ng of total RNA was used as input for the SMART-Seq v4 Ultra Low Input RNA kit (Takara Bio USA. Inc), which converts poly(A) RNA to full-length cDNA using a modified oligo (dT) primer with simultaneous cDNA amplification. The resulting double-stranded cDNA was then fragmented using a Covaris E210 system with the target size of 300bp. Libraries were prepared from fragmented double-stranded cDNA using an Illumina Stranded mRNA Prep Ligation kit (Illumina). For RNA obtained from 0.2 μm filters, ribosomal RNA was removed using a riboPOOL Seawater Kit (Galen Laboratory Supplies, North Haven, Connecticut, USA). The riboPOOL Seawater Kit is a customized mixture of Removal Solutions: Pan-Prokaryote riboPOOL, Pan-Plant riboPOOL and Pan-Mammal in a ratio of 6:1:1. The rRNA-depleted total

RNA was used for cDNA synthesis by Ovation RNA-Seq System V2 (TECAN, Redwood City, USA). Double stranded cDNA was then prepared for the libraries using an Illumina Stranded mRNA Prep Ligation kit (Illumina). Ampure XP beads (Beckman Coulter) were used for final library purification. Library quality was analyzed on a 2200 TapeStation System with an Agilent High Sensitivity DNA 1000 ScreenTape System (Agilent Technologies, Santa Clara, CA, USA). Resulting libraries were subjected to paired-end Illumina sequencing via NovaSeq S4.

The input paired-end fastq sequences are trimmed of sequencing adapters, primers and low quality bases by using either BLASTN (NCBI, v2.2.25) [79] or trimmomatic, v0.36 [80]. The trimmed paired and unpaired sequences were then depleted of rRNA sequences with riboPicker v0.4.3 [81]. The command-line program clc_assembler, v5.2.1 (Qiagen) was used to assemble processed sequences into contigs and ORFs were identified by FragGeneScan, v1.31 [82]. The trimmed sequences were mapped to the predicted ORFs using the command-line program clc_mapper, v5.2.1 (Qiagen) to generate mapped raw read counts for each ORF. The raw counts were normalized initially to RPKM values, to account for variations in inter-sample sequencing depth and the ORF sequence length [83]. The RPKM values were subsequently converted to TPM (transcripts per million) units for estimation of the relative RNA abundance among samples [84]. The ORFs were annotated for putative function by several programs in parallel using BLASTP against PhyloDB, hidden Markov models PFAM and TIGRFAM by HMMER, v3.3.2 [85], KEGG Ortholog HMM by kofamscan, v1.3.0 [86], and transmembrane HMM by TMHMM [87]. Additional annotations were generated by similarity searches using BLASTP to transporter (PhyloDB), organelle (PhyloDB) and KOG [88] databases. The ORFs are assigned to the best taxonomic species/group as determined by LPI (Lineage Probability Index) analysis [89]. The final list of

curated ORFs was generated by removing ORFs with low mapping coverage (<50 reads total over all samples) and with no BLAST hits and no known domains.

Statistical analysis and data visualization

ANOVA and Dunnett tests were performed using MATLAB 2019a. Statistics are summarized in Supplementary Table 3. The linear regression calculated for the relationship between ρZn and pCO_2 (Fig. 1h) is a two-way (type-II) linear regression, which allows for error in both the x and y parameters and do not assume dependence between the x and y axes. The two-way regression MATLAB function (lsqfitma.m) is available in python at https://github.com/rebecca-chmiel/GP15. Figures were made using matplotlib (version 3.5.0), Ocean Data View (version 5.5.2), Excel (2019), and RStudio (version 1.3.1093).

Data availability

CICLOPS (NBP18-01) total dissolved Zn, Zn uptake rates, macronutrients, and pigment datasets are available through the NSF's Biological and Chemical Oceanography Data Management Office (BCO-DMO) repository under project number 774945 (https://www.bco-dmo.org/project/774945). The mass spectrometry global proteomics data for CICLOPS bottle incubations and water column analyses have been deposited with the ProteomeXchange Consortium through the PRIDE repository under the project name "Zinc-iron co-limitation of natural marine phytoplankton assemblages in coastal Antarctica" with project accession number PXD037056 (https://www.ebi.ac.uk/pride/archive/projects/PXD037056). This data is accessible for review by using the following login information: username reviewer_pxd037056@ebi.ac.uk, password: lFdOUoEb. The translated transcriptome used for spectrum to peptide matching has

been deposited in the National Center for Biotechnology Information sequence read archive under BioProject accession no. PRJNA890306 (https://www.ncbi.nlm.nih.gov/bioproject/?term=PRJNA890306) and RNA-Seq BioSample accession nos. SAMN31286421-SAMN31286522 (https://www.ncbi.nlm.nih.gov/biosample/?term=SAMN31286421).

Acknowledgements

We thank the captain, crew, marine technicians and science party of RVIB Nathaniel B. Palmer for their support and contributions to the success of the NBP18-01 cruise. We thank Natalie Cohen for assistance and training with the seaFAST. We thank Veronique Oldham for assistance with trace metal sampling. This work was funded by the National Science Foundation (2123055, 2125063, 1643684, 1850719, 1924554 to M.A.S.; NSF-PLR 1643845 to R.B.D), and the National Institutes of Health (GM135709-01A1 to M.A.S).

Author contributions statement

All authors contributed to data acquisition and analysis. RMK, NLS, LEL, RJC, DR, DMM, MRM, FB, RBD, GRD and MAS implemented the shipboard incubation study. RMK, MMB, RJC, DR, TJH, and AVS contributed to formal analysis. NLS, LEL, FB, OM, RF, and GRD contributed to pigment datasets and interpretations. CB provided bacterial abundance data. RBD contributed DIC and *in situ* pCO_2 data. AVS contributed analyses and discussion regarding historical pCO_2 data. AEA contributed the meta transcriptome reference database used for proteomic analyses. RMK and MAS wrote the original draft. RMK, MAS, GRD, AVS, TJH, and RBD contributed to review and editing. All authors approved the final submitted manuscript.

Competing interests statement

The authors declare no competing interests.

References

1. Moore, C. M. *et al.* Processes and patterns of oceanic nutrient limitation. *Nat. Geosci.* **6**, 701–710 (2013).
2. Bruland, K. W. Oceanographic distributions of cadmium, zinc, nickel, and copper in the North Pacific. *Earth Planet. Sci. Lett.* **47**, 176–198 (1980).
3. Jakuba, R. W., Saito, M. A., Moffett, J. W. & Xu, Y. Dissolved zinc in the subarctic North Pacific and Bering Sea: Its distribution, speciation, and importance to primary producers. *Glob. Biogeochem. Cycles* (2012) doi:10.1029/2010GB004004.
4. Bruland, K. W. Complexation of zinc by natural organic ligands in the central North Pacific. *Limnol. Oceanogr.* **34**, 269–285 (1989).
5. Baars, O. & Croot, P. L. The speciation of dissolved zinc in the Atlantic sector of the Southern Ocean. *Deep Sea Res. Part II Top. Stud. Oceanogr.* **58**, 2720–2732 (2011).
6. Sunda, W. G. & Huntsman, S. A. Effect of Zn, Mn, and Fe on Cd accumulation in phytoplankton: Implications for oceanic Cd cycling. *Limnol. Oceanogr.* **45**, 1501–1516 (2000).
7. Saito, M. A., Goepfert, T. J. & Ritt, J. T. Some thoughts on the concept of colimitation: Three definitions and the importance of bioavailability. *Limnol. Oceanogr.* **53**, 276–290 (2008).

8. Lhospice, S. *et al.* Pseudomonas aeruginosa zinc uptake in chelating environment is primarily mediated by the metallophore pseudopaline. *Sci. Rep.* **7**, 17132 (2017).
9. Mazzotta, M. G. *et al*. Characterization of the metalloproteome of Pseudoalteromonas (BB2-AT2): biogeochemical underpinnings for zinc, manganese, cobalt, and nickel cycling in a ubiquitous marine heterotroph. *Metallomics* **13**, (2021).
10. Ye, N. *et al.* The role of zinc in the adaptive evolution of polar phytoplankton. *Nat. Ecol. Evol*. **6**, 965–978 (2022).
11. Scharek, R., Van Leeuwe, M. A. & De Baar, H. J. W. Responses of Southern Ocean phytoplankton to the addition of trace metals. *Deep-Sea Res. Part II Top. Stud. Oceanogr.* (1997) doi:10.1016/S0967-0645(96)00074-4.
12. Coale, K. H., Wang, X., Tanner, S. J. & Johnson, K. S. Phytoplankton growth and biological response to iron and zinc addition in the Ross Sea and Antarctic Circumpolar Current along 170°W. *Deep Sea Res. Part II Top. Stud. Oceanogr.* **50**, 635–653 (2003).
13. Ellwood, M. J. Zinc and cadmium speciation in subantarctic waters east of New Zealand. *Mar. Chem.* (2004) doi:10.1016/j.marchem.2004.01.005.
14. Crawford, D. W. *et al.* Influence of zinc and iron enrichments on phytoplankton growth in the northeastern subarctic Pacific. *Limnol. Oceanogr.* **48**, 1583–1600 (2003).
15. Franck, V., Bruland, K., Hutchins, D. & Brzezinski, M. Iron and zinc effects on silicic acid and nitrate uptake kinetics in three high-nutrient, low-chlorophyll (HNLC) regions. *Mar. Ecol. Prog. Ser.* **252**, 15–33 (2003).
16. Dreux Chappell, P. *et al.* Preferential depletion of zinc within Costa Rica upwelling dome creates conditions for zinc co-limitation of primary production. *J. Plankton Res.* **38**, 244–255 (2016).

17. Salisbury, J. E. *et al.* Seasonal observations of surface waters in two Gulf of Maine estuary-plume systems: Relationships between watershed attributes, optical measurements and surface pCO2. *Estuar. Coast. Shelf Sci.* **77**, 245–252 (2008).
18. Chen, S. *et al.* A machine learning approach to estimate surface ocean pCO2 from satellite measurements. *Remote Sens. Environ.* **228**, 203–226 (2019).
19. Cai, W.-J. *et al.* Controls on surface water carbonate chemistry along North American ocean margins. *Nat. Commun.* **11**, 2691 (2020).
20. Morel, F. M. M., Lam, P. J. & Saito, M. A. Trace metal substitution in marine phytoplankton. *Annu. Rev. Earth Planet. Sci.* **48**, 491–517 (2020).
21. Cullen, J. T., Lane, T. W., Morel, F. M. M. & Sheerell, R. M. Modulation of cadmium uptake in phytoplankton by seawater CO2 concentration. *Nature* (1999) doi:10.1038/46007.
22. Cullen, J. T. & Sherrell, R. M. Effects of dissolved carbon dioxide, zinc, and manganese on the cadmium to phosphorus ratio in natural phytoplankton assemblages. *Limnol. Oceanogr.* **50**, 1193–1204 (2005).
23. Morel, F. M. M. *et al.* Zinc and carbon co-limitation of marine phytoplankton. *Nature* **369**, 740–742 (1994).
24. Sunda, W. G. & Huntsman, S. A. Effect of CO 2 supply and demand on zinc uptake and growth limitation in a coastal diatom. *Limnol. Oceanogr.* **50**, 1181–1192 (2005).
25. Price, N. M. & Morel, F. M. M. Cadmium and cobalt substitution for zinc in a marine diatom. *Nature* **344**, 658–660 (1990).
26. Kellogg, R. M. *et al.* Efficient zinc/cobalt inter□replacement in northeast Pacific diatoms and relationship to high surface dissolved Co□: Zn ratios. *Limnol. Oceanogr.* **65**, 2557–2582 (2020).

27. Lane, T. W. & Morel, F. M. A biological function for cadmium in marine diatoms. *Proc. Natl. Acad. Sci. U. S. A.* **97**, 4627–31 (2000).

28. Jensen, E. L., Clement, R., Kosta, A., Maberly, S. C. & Gontero, B. A new widespread subclass of carbonic anhydrase in marine phytoplankton. *ISME J.* **13**, 2094–2106 (2019).

29. Arrigo, K. R., Lowry, K. E. & van Dijken, G. L. Annual changes in sea ice and phytoplankton in polynyas of the Amundsen Sea, Antarctica. *Deep Sea Res. Part II Top. Stud. Oceanogr.* **71–76**, 5–15 (2012).

30. Arrigo, K. R., van Dijken, G. & Long, M. Coastal Southern Ocean: A strong anthropogenic CO2 sink. *Geophys. Res. Lett.* (2008) doi:10.1029/2008GL035624.

31. DeJong, H. B. & Dunbar, R. B. Air-Sea CO2 Exchange in the Ross Sea, Antarctica. *J. Geophys. Res. Oceans* **122**, 8167–8181 (2017).

32. Martin, J. H., Fitzwater, S. E. & Gordon, R. M. Iron deficiency limits phytoplankton growth in Antarctic waters. *Glob. Biogeochem. Cycles* **4**, 5–12 (1990).

33. Sedwick, P. N. *et al.* Early season depletion of dissolved iron in the Ross Sea polynya: Implications for iron dynamics on the Antarctic continental shelf. *J. Geophys. Res.* **116**, C12019 (2011).

34. Bertrand, E. M. *et al.* Vitamin B 12 and iron colimitation of phytoplankton growth in the Ross Sea. *Limnol. Oceanogr.* **52**, 1079–1093 (2007).

35. Burns, S. M. *et al.* Interactions of bioactive trace metals in shipboard Southern Ocean incubation experiments. *Limnol. Oceanogr.* **68**, 525–543 (2023).

36. Smith, W. O. *et al.* Interannual variations in nutrients, net community production, and biogeochemical cycles in the Ross Sea. *Deep-Sea Res. Part II Top. Stud. Oceanogr.* (2006) doi:10.1016/j.dsr2.2006.02.014.

37. Mangoni, O. *et al*. Phaeocystis antarctica unusual summer bloom in stratified antarctic coastal waters (Terra Nova Bay, Ross Sea). *Mar. Environ. Res.* (2019) doi:10.1016/j.marenvres.2019.05.012.

38. DiTullio, G. R. & Smith, W. O. Spatial patterns in phytoplankton biomass and pigment distributions in the Ross Sea. *J. Geophys. Res. Oceans* **101**, 18467–18477 (1996).

39. Fitzwater, S. E., Johnson, K. S., Gordon, R. M., Coale, K. H. & Smith, W. O. Trace metal concentrations in the Ross Sea and their relationship with nutrients and phytoplankton growth. *Deep-Sea Res. Part II Top. Stud. Oceanogr.* **47**, 3159–3179 (2000).

40. Kellogg, R. M. Assessing the potential for Zn limitation of marine primary production: proteomic characterization of the low Zn stress response in marine diatoms. (Massachusetts Institute of Technology; the Woods Hole Oceanographic Institution, 2022).

41. Saito, M. A. & Goepfert, T. J. Zinc-cobalt colimitation of *Phaeocystis antarctica*. *Limnol. Oceanogr.* **53**, 266–275 (2008).

42. Chmiel, R. J. *et al*. *Low Cobalt Inventories in the Amundsen and Ross Seas Driven by High Demand for Labile Cobalt Uptake Among Native Phytoplankton Communities*. https://egusphere.copernicus.org/preprints/2023/egusphere-2023-402/ (2023) doi:10.5194/egusphere-2023-402.

43. Sperfeld, E., Raubenheimer, D. & Wacker, A. Bridging factorial and gradient concepts of resource co-limitation: towards a general framework applied to consumers. *Ecol. Lett.* **19**, 201–215 (2016).

44. Kellogg, R. M. *et al.* Adaptive responses of marine diatoms to zinc scarcity and ecological implications. *Nat. Commun. 2022 131* **13**, 1–13 (2022).

45. Allen, A. E. *et al.* Whole-cell response of the pennate diatom Phaeodactylum tricornutum to iron starvation. *Proc. Natl. Acad. Sci.* **105**, 10438–10443 (2008).

46. Behnke, J. & LaRoche, J. Iron uptake proteins in algae and the role of Iron Starvation-Induced Proteins (ISIPs). *Eur. J. Phycol.* **55**, 339–360 (2020).

47. Bertrand, E. M. *et al.* Iron limitation of a springtime bacterial and phytoplankton community in the ross sea: implications for vitamin b(12) nutrition. *Front. Microbiol.* **2**, 160 (2011).

48. DiTullio, G. R., Garcia, N., Riseman, S. F. & Sedwick, P. N. Effects of iron concentration on pigment composition in Phaeocystis antarctica grown at low irradiance. *Biogeochemistry* **83**, 71–81 (2007).

49. Milner, M. J., Seamon, J., Craft, E. & Kochian, L. V. Transport properties of members of the ZIP family in plants and their role in Zn and Mn homeostasis. *J. Exp. Bot.* **64**, 369–381 (2013).

50. Bender, S. J. *et al.* Colony formation in Phaeocystis antarctica: connecting molecular mechanisms with iron biogeochemistry. *Biogeosciences* **15**, 4923–4942 (2018).

51. Jensen, E. L., Maberly, S. C. & Gontero, B. Insights on the Functions and Ecophysiological Relevance of the Diverse Carbonic Anhydrases in Microalgae. *Int. J. Mol. Sci.* **21**, 2922 (2020).

52. Kellogg, R. M. *et al.* Lack of a Zn/Co substitution ability in the polar diatom *Chaetoceros neogracile* RS19. *Limnol. Oceanogr.* **67**, 2265–2280 (2022).

53. Lane, T. W. & Morel, F. M. M. Regulation of Carbonic Anhydrase Expression by Zinc, Cobalt, and Carbon Dioxide in the Marine Diatom Thalassiosira weissflogii. *Plant Physiol.* **123**, 345–352 (2000).

54. Subhas, A. V., Adkins, J. F., Dong, S., Rollins, N. E. & Berelson, W. M. The carbonic anhydrase activity of sinking and suspended particles in the North Pacific Ocean. *Limnol. Oceanogr.* **65**, 637–651 (2019).

55. Jiang, L. *et al.* Global Surface Ocean Acidification Indicators From 1750 to 2100. *J. Adv. Model. Earth Syst.* **15**, e2022MS003563 (2023).

56. Cutter, G. A. & Bruland, K. W. Rapid and noncontaminating sampling system for trace elements in global ocean surveys. *Limnol. Oceanogr. Methods* (2012) doi:10.4319/lom.2012.10.425.

57. Takahashi, T., Sutherland, S. C. & Kozyr, A. Global Ocean Surface Water Partial Pressure of CO2 Database (LDEO Database Version 2019): Measurements Performed During 1957-2019 (NCEI Accession 0160492). *NOAA Natl. Cent. Environ. Inf.* (2020).

58. Dickson, A. G., Sabine, C. L. & Christian, J. R. *Guide to best practices for ocean CO2 measurement.* https://repository.oceanbestpractices.org/handle/11329/249 (2007) doi:10.25607/OBP-1342.

59. DeJong, H. B., Dunbar, R. B., Mucciarone, D. & Koweek, D. A. Carbonate saturation state of surface waters in the Ross Sea and Southern Ocean: controls and implications for the onset of aragonite undersaturation. *Biogeosciences* **12**, 6881–6896 (2015).

60. Van Heuven, S., Pierrot, D., Rae, J. W. B., Lewis, E. & Wallace, D. W. R. MATLAB Program Developed for CO2 System Calculations. ORNL/CDIAC-105b. (2011) doi:10.3334/CDIAC/OTG.CO2SYS_MATLAB_V1.1.

61. Sulpis, O., Lauvset, S. K. & Hagens, M. Current estimates of K1* and K2* appear inconsistent with measured CO2 system parameters in cold oceanic regions. *Ocean Sci.* **16**, 847–862 (2020).

62. Keeling, C. D. *et al.* Atmospheric carbon dioxide variations at Mauna Loa Observatory, Hawaii. *Tellus Dyn. Meteorol. Oceanogr.* **28**, 538 (1976).

63. Etheridge, D. M. *et al.* Natural and anthropogenic changes in atmospheric CO_2 over the last 1000 years from air in Antarctic ice and firn. *J. Geophys. Res. Atmospheres* **101**, 4115–4128 (1996).

64. Buitenhuis, E. T., Timmermans, K. R. & de Baar, H. J. W. Zinc-bicarbonate colimitation of Emiliania huxleyi. *Limnol. Oceanogr.* **48**, 1575–1582 (2003).

65. Riebesell, U., Wolf-Gladrow, D. A. & Smetacek, V. Carbon dioxide limitation of marine phytoplankton growth rates. *Nature* **361**, 249–251 (1993).

66. Sharp, J. D. *et al.* CO2SYSv3 for MATLAB. (2023) doi:10.5281/ZENODO.3950562.

67. Krumhardt, K. M., Lovenduski, N. S., Iglesias-Rodriguez, M. D. & Kleypas, J. A. Coccolithophore growth and calcification in a changing ocean. *Prog. Oceanogr.* **159**, 276–295 (2017).

68. Sunda, W. G. & Huntsman, S. A. Cobalt and zinc interreplacement in marine phytoplankton: Biological and geochemical implications. *Limnol. Oceanogr.* **40**, 1404–1417 (1995).

69. Wyatt, N. J. *et al.* Biogeochemical cycling of dissolved zinc along the GEOTRACES South Atlantic transect GA10 at 40°S. *Glob. Biogeochem. Cycles* **28**, 44–56 (2014).

70. Cohen, N. R. *et al.* Hydrothermal trace metal release and microbial metabolism in the northeastern Lau Basin of the South Pacific Ocean. *Biogeosciences* **18**, 5397–5422 (2021).

71. Rapp, I., Schlosser, C., Rusiecka, D., Gledhill, M. & Achterberg, E. P. Automated preconcentration of Fe, Zn, Cu, Ni, Cd, Pb, Co, and Mn in seawater with analysis using high-resolution sector field inductively-coupled plasma mass spectrometry. *Anal. Chim. Acta* (2017) doi:10.1016/j.aca.2017.05.008.

72. Wuttig, K. *et al.* Critical evaluation of a seaFAST system for the analysis of trace metals in marine samples. *Talanta* (2019) doi:10.1016/j.talanta.2019.01.047.

73. DiTullio, G. R., Geesey, M. E., Leventer, A. & Lizotte, M. P. Algal pigment ratios in the Ross Sea: Implications for Chemtax analysis of Southern Ocean data. in 35–51 (2003). doi:10.1029/078ARS03.

74. Schanke, N. L. *et al.* Biogeochemical and ecological variability during the late summer–early autumn transition at an ice-floe drift station in the Central Arctic Ocean. *Limnol. Oceanogr.* (2021) doi:10.1002/lno.11676.

75. Balestra, C., Alonso-Sáez, L., Gasol, J. M. & Casotti, R. Group-specific effects on coastal bacterioplankton of polyunsaturated aldehydes produced by diatoms. *Aquat. Microb. Ecol.* (2011) doi:10.3354/ame01486.

76. Cox, A. D., Noble, A. E. & Saito, M. A. Cadmium enriched stable isotope uptake and addition experiments with natural phytoplankton assemblages in the Costa Rica Upwelling Dome. *Mar. Chem.* **166**, 70–81 (2014).

77. Hughes, C. S. *et al.* Ultrasensitive proteome analysis using paramagnetic bead technology. *Mol. Syst. Biol.* **10**, 757 (2014).

78. Zhang, Y., Wen, Z., Washburn, M. P. & Florens, L. Refinements to Label Free Proteome Quantitation: How to Deal with Peptides Shared by Multiple Proteins. *Anal. Chem.* **82**, 2272–2281 (2010).

79. Altschul, S. F., Gish, W., Miller, W., Myers, E. W. & Lipman, D. J. Basic local alignment search tool. *J. Mol. Biol.* (1990) doi:10.1016/S0022-2836(05)80360-2.

80. Bolger, A. M., Lohse, M. & Usadel, B. Trimmomatic: a flexible trimmer for Illumina sequence data. *Bioinformatics* **30**, 2114–2120 (2014).

81. Schmieder, R., Lim, Y. W. & Edwards, R. Identification and removal of ribosomal RNA sequences from metatranscriptomes. *Bioinformatics* **28**, 433–435 (2012).
82. Rho, M., Tang, H. & Ye, Y. FragGeneScan: predicting genes in short and error-prone reads. *Nucleic Acids Res.* **38**, e191–e191 (2010).
83. Mortazavi, A., Williams, B. A., McCue, K., Schaeffer, L. & Wold, B. Mapping and quantifying mammalian transcriptomes by RNA-Seq. *Nat. Methods* **5**, 621–628 (2008).
84. Li, B. & Dewey, C. N. RSEM: accurate transcript quantification from RNA-Seq data with or without a reference genome. *BMC Bioinformatics* **12**, 323 (2011).
85. Eddy, S. R. Accelerated Profile HMM Searches. *PLoS Comput. Biol.* **7**, e1002195 (2011).
86. Aramaki, T. *et al.* KofamKOALA: KEGG Ortholog assignment based on profile HMM and adaptive score threshold. *Bioinformatics* **36**, 2251–2252 (2020).
87. Krogh, A., Larsson, B., von Heijne, G. & Sonnhammer, E. L. L. Predicting transmembrane protein topology with a hidden markov model: application to complete genomes11Edited by F. Cohen. *J. Mol. Biol.* **305**, 567–580 (2001).
88. Tatusov, R. L. *et al.* The COG database: an updated version includes eukaryotes. *BMC Bioinformatics* **4**, 41 (2003).
89. Podell, S. & Gaasterland, T. DarkHorse: a method for genome-wide prediction of horizontal gene transfer. *Genome Biol*. **8**, R16 (2007).
90. Chmiel, R. *et al*. Major processes of the dissolved cobalt cycle in the North and equatorial Pacific Ocean. *Biogeosciences* **19**, 2365–2395 (2022).

Main Text Figures and Tables

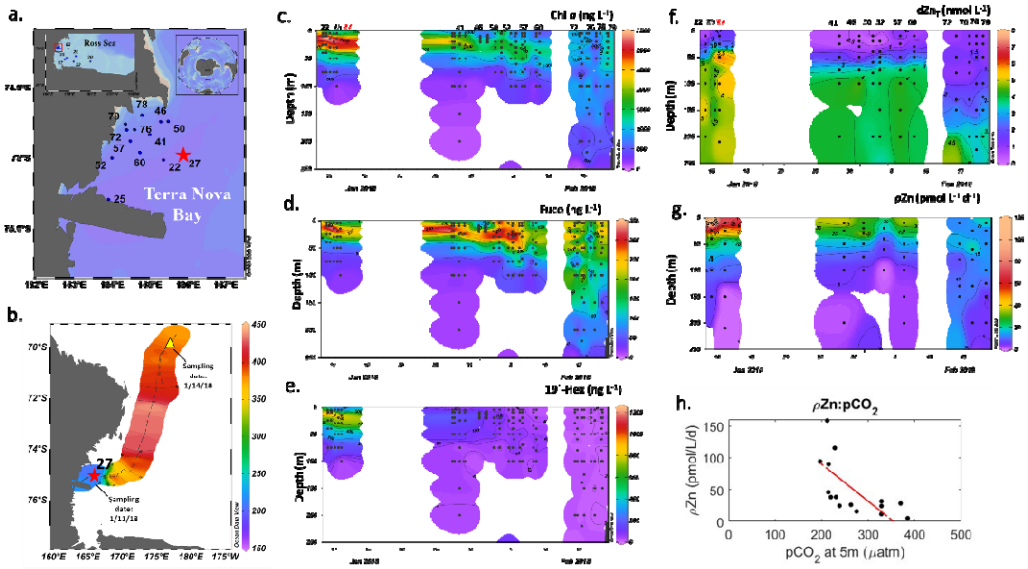

Figure 1. **Temporal biogeochemistry of Terra Nova Bay, Jan-Feb 2018.** (**a**) Sampling locations over the Ross Sea shelf in Terra Nova Bay, Antarctica. (**b**) Location of station 27 and surrounding seawater pCO_2 measured over a three-day transit northwards represented in color scale. Locations sampled on January 11, 2018 and on January 14, 2018 are indicated. (**c**) chlorophyll *a* (chl *a*), (**d**) fucoxanthin (fuco), (**e**) 19' hexanoyloxyfucoxanthin (19'-hex), (**f**) total dissolved Zn (dZn_T), and (**g**) total Zn uptake rates for all Terra Nova Bay stations over time measured in the upper 250m. Station numbers are given at the top of (c) and (f). Station data is presented in order of sampling date, from the earliest (Stn 22, early January) to the latest (Stn 79, late February). (**h**) negative linear relationship between seawater CO_2 partial pressure (pCO_2) at 5 m depth and Zn uptake rates (ρZn) measured at surface (≤ 10m) depths for 15 stations of the CICLOPS cruise (n = 15, R^2 = 0.63). The data gap between January 13-23 occurred when the ship was unable to sample due to icebreaking duties for the McMurdo Station resupply ship. Stations indicated in (a) are those where the trace metal rosette (TMR) was deployed; pigment data was supplemented with additional stations using a CTD.

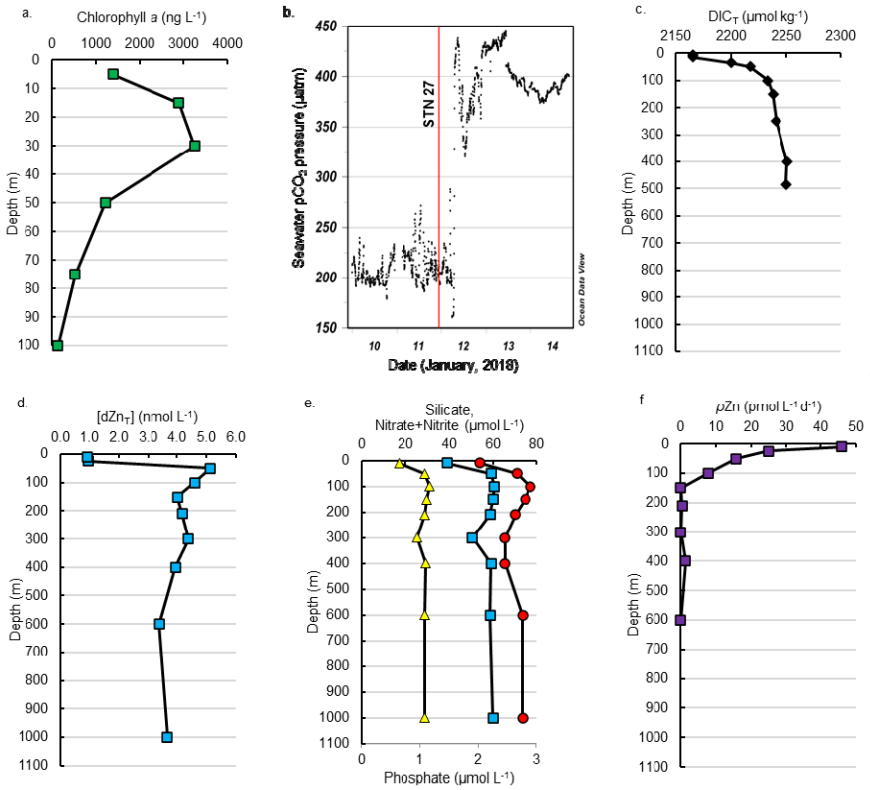

Figure 2. **Water column biogeochemistry at the experimental site. (a)** chlorophyll a within the upper 100 m. (**b**), pCO_2 measured over time within TNB during a 3-day transit. The vertical red line denotes the pCO_2 level at the time of initial seawater collection at station 27. Depth profiles of (**c**) total dissolved inorganic carbon (DIC_T), (**d**) total dissolved Zn (dZn_T), (**e**) the macronutrients nitrate+nitrite (N+N), phosphate (P), and silicate (Si), and (**f**) total Zn uptake rates.

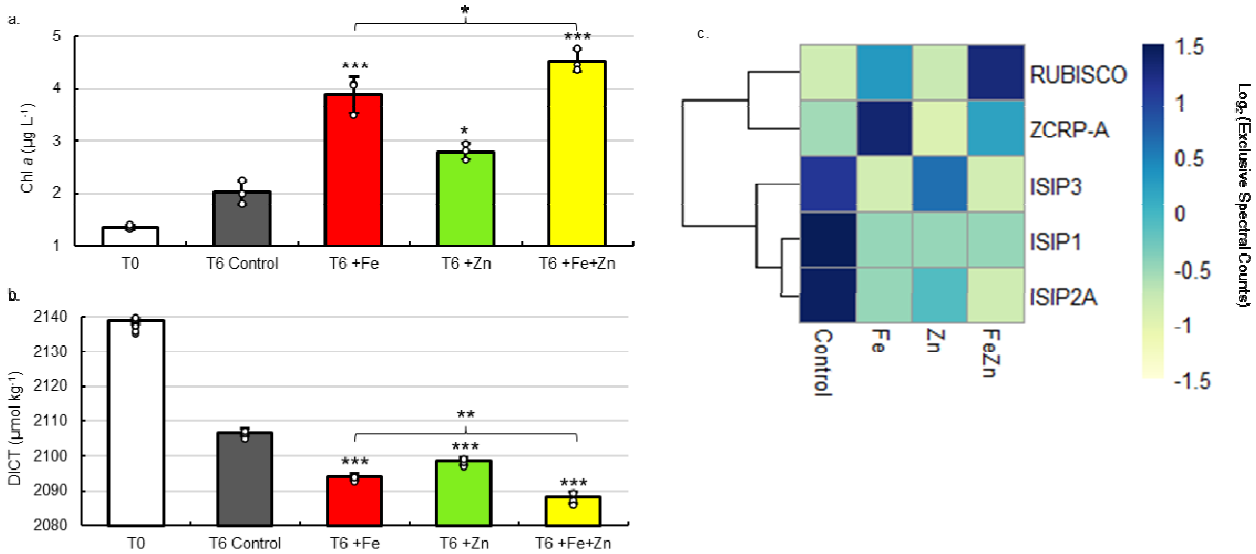

Figure 3. Evidence for Zn co-limitation with Fe in bottle incubations. (**a**) Chlorophyll *a* and (**b**) total salinity-normalized DIC in each treatment at T6. Significant differences among groups were found using one-way ANOVA and post-hoc Dunnett test (*** $p < 0.001$, ** $p < 0.01$, * $p < 0.05$). Error bars are the standard deviation of biological triplicates (n=3). Individual data points are overlaid (white circles). (**c**) Heatmap of log2 exclusive protein spectral counts showing relative protein abundance at the KOG annotation level. The dendrogram shows similarity in spectral abundance among samples based on Euclidean distance and hierarchical clustering. Each row represents a KOG annotation. Spectral counts associated with identical KOG descriptions were summed together. Color gradients represent low (yellow) to high (blue) protein expression. Ribulose-1,5-biphosphate carboxylase/oxygenase (RUBISCO), zinc/cobalt responsive protein A (ZCRP-A), and iron starvation induced proteins (ISIP1, ISIP2A, ISIP3) are shown.

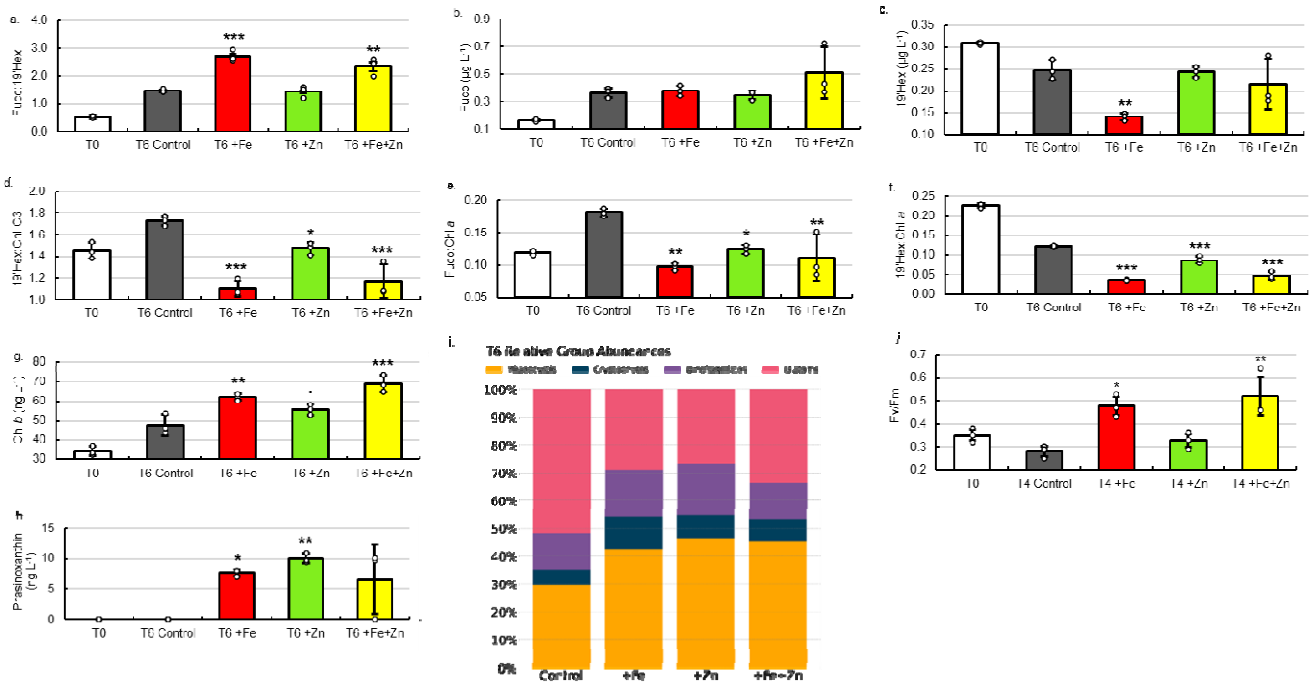

Figure 4. Pigment analysis of T6 incubations. (**a**) ratio of fucoxanthin: 19'-Hex, (**b**) fucoxanthin, (**c**) 19-hexanoyloxyfucoxanthin (19'-Hex), (**d**) ratio of 19'-Hex: chl c3, (**e**) ratio of fucoxanthin: chlorophyll *a*, (**f**) ratio of 19'-Hex: chlorophyll *a*, (**g**) chlorophyll *b*, (**h**) prasinoxanthi, (**i**) relative abundances of *Phaeocystis*, cryptophytes, dinoflagellates, and diatoms as estimated by total protein spectral counts in T6 incubations (see Methods), and (**j**) maximum quantum efficiency (Fv/Fm) among treatments at T4. Significant differences among groups were found using one-way ANOVA and post-hoc Dunnett test (*** $p < 0.001$, ** $p < 0.01$, * $p < 0.05$, . $p < 0.1$). Data with error bars are presented as mean values ± the standard deviation of biological triplicates (n=3) with individual data points overlaid (white circles).

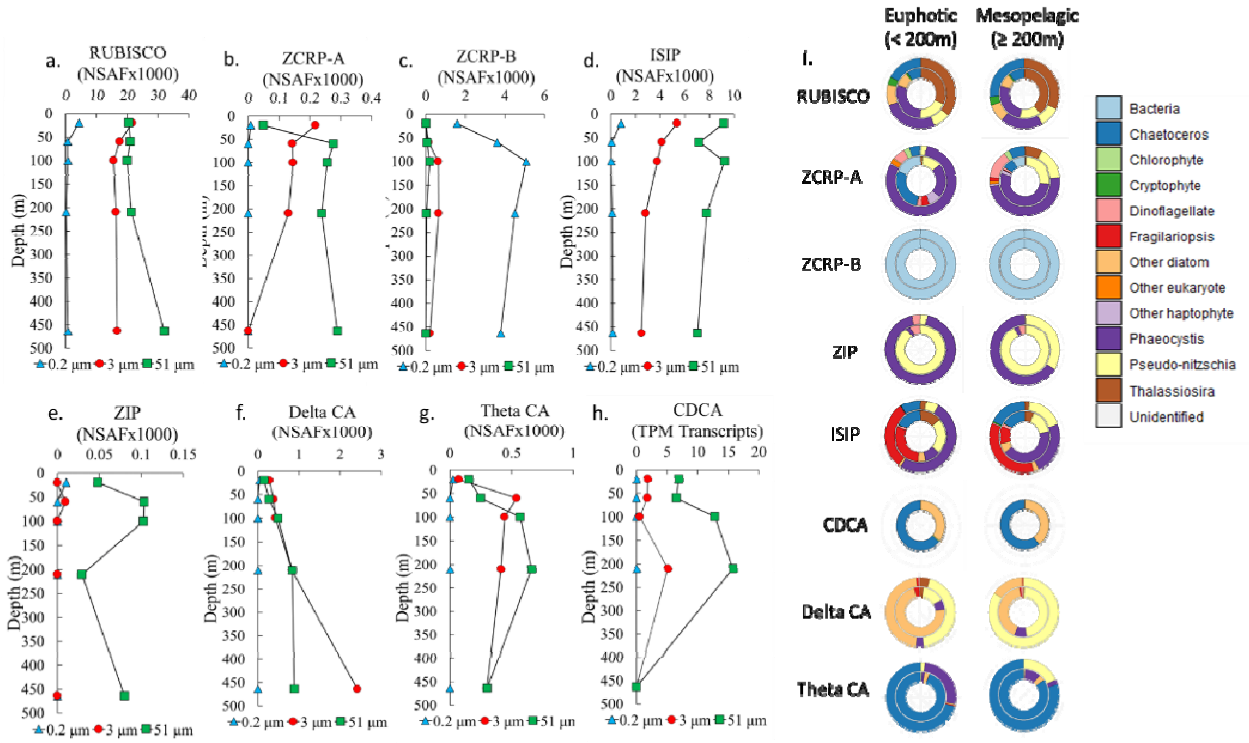

Figure 5. Metatranscriptomic and metaproteomic detection of Zn- and Fe-related proteins of interest at station 27. Depth profiles of summed NSAF-normalized protein spectral counts of (**a**) RUBISCO, (**b**) ZCRP-A, (**c**) ZCRP-B, (**d**) iron starvation induced proteins (ISIPs), (**e**) ZIP, (**f**) Delta CA, and (**g**) Theta CA for each size fraction (0.2, 3 and 51µm). (**h**) TPM-normalized transcript read counts of CDCA. (**i**) stacked pie charts depicting relative community composition for proteins of interest for euphotic (< 200 m) and mesopelagic (≥ 200 m) depths. The outer rings show community composition based on NSAF-normalized protein spectral counts while the inner rings are TPM-normalized transcript read counts. Proteins and transcripts in (i) were summed across all size fractions. ISIPs are the combined spectral counts of ISIP1A, ISIP2A and ISIP3.

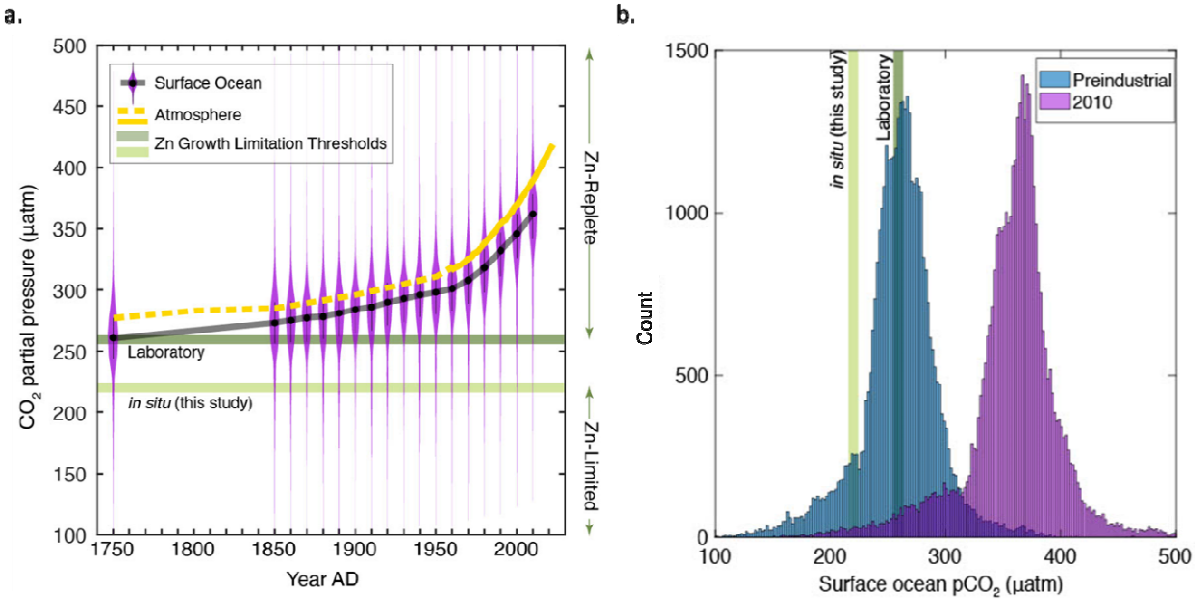

Figure 6. **The partial pressure of CO_2 (pCO_2) and associated phytoplankton responses from this study and the literature**. **(a)** Pre-industrial and decadal surface ocean pCO_2 reconstructions plotted as violin plots, with a running black line through the median values. The atmospheric curve is a composite of ice core data (dashed yellow line[63]) and the Mauna Loa record (solid yellow line[62]). Thresholds for zinc-limited growth are plotted as the median of previous laboratory results (259 µatm, dark green line; see Methods), and estimated from the *in situ* results of this study (220 µatm, light green line). **(b)** Data in (a) plotted as a histogram comparing preindustrial and modern (2010) pCO_2 values, with the same Zn growth limitation thresholds indicated.